

pubs.acs.org/JACS Article

Photochemical Dearomative Cycloadditions of Quinolines and Alkenes: Scope and Mechanism Studies

Renyu Guo, Souvik Adak, Peter Bellotti, Xinfeng Gao, W. Walker Smith, Sam Ngan Le, Jiajia Ma, K. N. Houk,* Frank Glorius,* Shuming Chen,* and M. Kevin Brown*



Cite This: J. Am. Chem. Soc. 2022, 144, 17680-17691



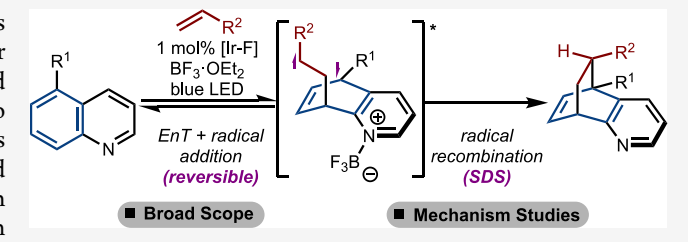
ACCESS I

III Metrics & More

Article Recommendations

s Supporting Information

ABSTRACT: Photochemical dearomative cycloaddition has emerged as a useful strategy to rapidly generate molecular complexity. Within this context, stereo- and regiocontrolled intermolecular *para*-cycloadditions are rare. Herein, a method to achieve photochemical cycloaddition of quinolines and alkenes is shown. Emphasis is placed on generating sterically congested products and reaction of highly substituted alkenes and allenes. In addition, the mechanistic details of the process are studied, which revealed a reversible radical addition and a selectivity-determining radical recombination. The region and stereochemical outcome of



radical recombination. The regio- and stereochemical outcome of the reaction is also rationalized.

■ INTRODUCTION

Cycloaddition reactions are among the most efficient and atomeconomical approaches to quickly build up molecular complexity. Arene—alkene cycloaddition (AAC) reactions represent an ideal means of converting planar arenes into three-dimensional architectures. However, most thermally induced dearomative cycloadditions are difficult to realize experimentally due to high kinetic barriers and competing reverse processes. Photochemically driven processes have allowed for the development of AAC as a photon allows for the reaction to proceed via excited-state intermediates.

Photochemical cycloadditions between arenes and unsaturated systems (typically alkenes and acetylenes) can lead to the formation of *ortho, meta,* and *para* regioisomeric products (Scheme 1A).⁴ Under direct irradiation, the singlet S₁ excited state of the arene is generated, and the formation of *meta*-cycloadducts dominates via a concerted cycloaddition.⁵ However, if the triplet T₁ excited state is generated, arenes can behave more like diradicals, allowing access to *ortho* and *para* adducts via stepwise radical cycloaddition. Computational studies by Houk established this general paradigm,⁶ which was further confirmed by Cornelisse and co-workers.⁷ As the S₁ excited state of the arene can be easily accessed with simple UV-light irradiation, *meta* cycloadditions have been extensively studied and applied in the synthesis of various natural products.^{3b,8,9}

Efficient access to the T_1 state of the arene through direct excitation is challenging for several reasons. First, the gap between S_0 and S_1 can be large, especially for S_1 ($\pi-\pi^*$). As a result, short-wavelength irradiation with Hg lamps is usually required. Second, the transition from S_1 to T_1 may be difficult because of the relatively fast relaxation of S_1 to the ground state.

Third, in accordance with El-Sayed's rule, a forbidden ISC would be necessary for the conversion of S_1 $(\pi-\pi^*)$ to T_1 $(\pi-\pi^*)$. Finally, since *meta* cycloaddition can easily proceed via the S_1 state, there will likely be a competition among multiple cycloaddition pathways even if the T_1 state can be accessed. Despite these challenges, several *ortho*- and *para*-cycloadditions have been developed. For example, ortho-cycloadditions have been reported for systems in which the ISC to the T_1 $(\pi-\pi^*)$ is facile. However, these systems are limited to specialized substrates with tethered alkenes. Recently, developments have been made with phenanthrene derivatives in an intramolecular cycloaddition. Only a few examples showed that electron-poor naphthalene derivatives could react with electron-deficient alkenes to yield the *para* cycloadducts.

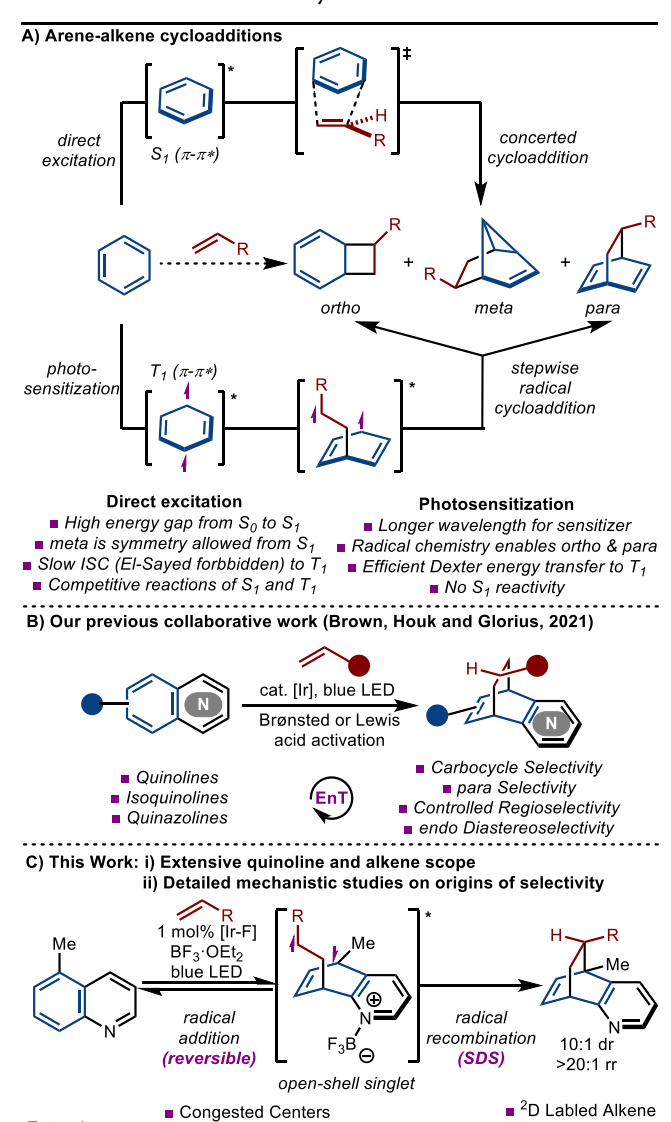
An alternative method to access the T₁ state of the arene is by visible-light mediated triplet—triplet energy transfer (EnT). ¹⁵ Because the T₁ state is accessed directly without having to generate S₁, only stepwise *ortho*-and *para*-cycloadditions are observed. Examples of EnT-induced dearomative *ortho*-cycloadditions include reactions of indoles ¹⁶ as reported by You, ¹⁷ Oderinde, ¹⁸ Fu, ¹⁹ and Zhang. ²⁰ In addition, early work from Meggers demonstrated the dearomatization of benzofuran and benzothiophene. ²¹ Oderinde and co-workers later applied this strategy to electron-deficient indoles, benzofurans, benzothiophenes, and azaindoles. ²² Glorius also realized the *ortho*

Received: July 21, 2022 Published: September 15, 2022





Scheme 1. Arene-Alkene Cycloaddition



cycloaddition of benzothiophene via an endergonic EnT.²³ para-Cycloaddition is still rare under EnT conditions and mainly focuses on the sensitization of alkenes instead of arenes.²⁴

Disubstituted Alkenes

Allenes

Mechanistic

Studies

¹³C KIE Study

■ DFT Calculations

Extensive

Recently, our groups developed a selective intermolecular para-cycloaddition of bicyclic azaarenes with various activated and unactivated alkenes initiated by EnT (Scheme 1B). 25 This reaction displays good selectivity toward the formation of one isomer and affords valuable functionalized aromatic heterocycles that have been established as privileged motifs in pharmaceutically active compounds.²⁶ Additional studies revealed a novel photochemical cascade with certain substitution patterns.²⁷ In this study, we greatly expand upon the substrate scope to more challenging examples such as disubstituted alkenes and allenes under Lewis acid-mediated conditions developed in the Brown lab (Scheme 1C). In addition, we demonstrate that targets containing tetrasubstituted carbons can be accessed readily using this protocol. Finally, through a combination of mechanistic experiments and density functional theory (DFT) calculations, we present a detailed analysis of the reaction

mechanism and reveal the energy landscape of the transformation.

RESULTS AND DISCUSSION

Initially, we employed 2-*i*Pr-thioxanthone (ITX, $E_T = 65.4$ kcal/ mol)²⁸ as the photosensitizer for the reaction between quinoline $(E_{\rm T}=61.9~{\rm kcal/mol})$ and 1-hexene, which resulted in <2% conversion. A similar result was obtained with [Ir- $(dFCF_3ppy)_2dtbbpy]PF_6$ (Ir-F, $E_T = 60.1$ kcal/mol). Addition of 25 mol % HNTf2 resulted in the formation of the para cycloadducts 2 and 3, albeit in low yields (Table 1, entry 3).

Table 1. Reaction Optimization



entry ^a	photosensitizer	E _T (kcal/mol)	acids	yield (%) ^b
1	2- <i>i</i> Pr-thioxanthone ^c	65.4	-	<2
2	[lr(dFCF ₃ ppy) ₂ dtbbpy]PF ₆	60.1	-	<2
3	$[{\rm Ir}({\rm dFCF_3ppy})_2{\rm dtbbpy}]{\rm PF_6}$	60.1	25 mol % HNTf ₂	~10
4	$[Ir(dFCF_3ppy)_2dtbbpy]PF_6$	60.1	25 mol % Sc(OTf) ₃	26
5	$[Ir(dFCF_3ppy)_2dtbbpy]PF_6$	60.1	25 mol % $\mathrm{BF_3}{\cdot}\mathrm{OEt_2}$	24
6	[lr(dFCF ₃ ppy) ₂ dtbbpy]PF ₆	60.1	125 mol % BF ₃ ·OEt ₂	>95
7	2-i-Pr-thioxanthone ^c	65.4	125 mol % BF ₃ ·OEt ₂	>95
8	[Ir(dFppy) ₂ dtbbpy]PF ₆	57.1	125 mol % BF ₃ ·OEt ₂	33
9	fac-Ir(ppy) ₃	55.2	125 mol % BF ₃ ·OEt ₂	<2

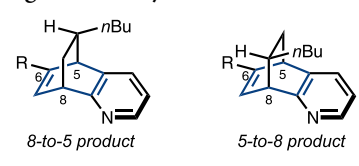
^aReactions were run on a 0.1 mmol scale. ^bCombined yields (rr and dr) were determined by crude NMR for using CH2Br2 as the internal standard. ^c5 mol % cat., 395 nm LED, 36 h.

Further studies showed that Lewis acids were more effective (Table 1, entries 4–5). We found that 125 mol % $BF_3 \cdot OEt_2$ was required for full conversion (Table 1, entry 6), likely due to product inhibition. Finally, while the higher-energy sensitizer ITX gave a similar result as [Ir(dFCF₃ppy)₂dtbbpy]PF₆ (Table 1, entry 7), the use of lower-energy sensitizers led to diminished yields.

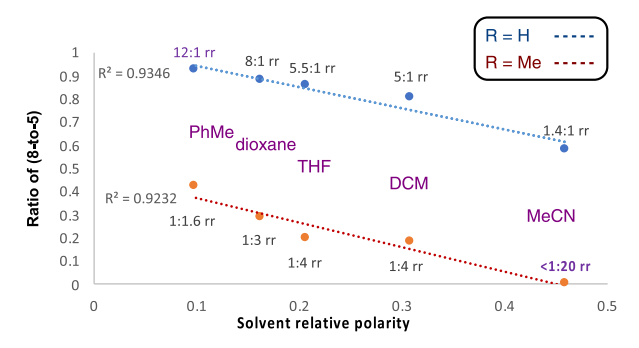
While evaluation of various Lewis acids, photosensitizers, and temperatures did not alter the selectivities, regioselectivity was found to be controlled by the polarity of the solvent and the position of the quinoline substituent (Scheme 2A). For these reactions, we define 2 as the 8-to-5 product and 3 as the 5-to-8 product based on the order of bond formation (vide infra). For quinoline (1), the 8-to-5 product 2 was the major regioisomer formed in all solvents evaluated, with the highest regioselectivity observed in toluene (12:1 rr). When 6-Me-quinoline was evaluated, a switch in regioselectivity occurred, yielding the 5-to-8 product as the major isomer. In addition, a similar correlation between regioselectivity and solvent polarity was observed, with MeCN yielding the highest regioselectivity for the 5-to-8 product (>20:1 rr).²

To understand the impact of substituent position on regioselectivity, we tested quinolines with methyl groups at different positions (Scheme 2B).^{30,31} For quinolines with substitution on the pyridine ring (products 2, 4-7) or substitution on the 5- and 7-positions of the phenyl ring (products 8-9), the 8-to-5 product was favored. The 5-to-8

Scheme 2. Regioselectivity

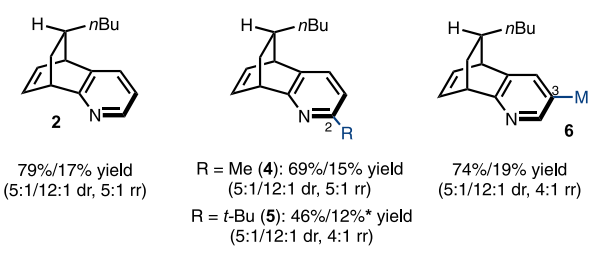


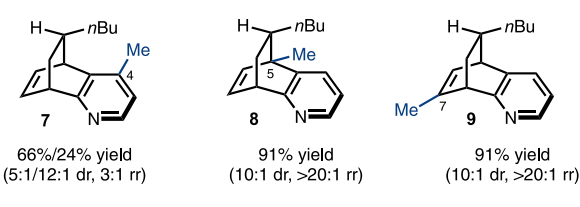
(A) Solvent controlled regioselectivity



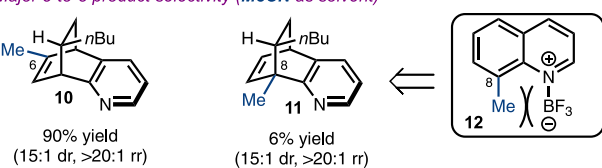
(B) Substrate controlled regioselectivity

Major 8-to-5 product selectivity (DCM as solvent)





Major 5-to-8 product selectivity (MeCN as solvent)



X-ray structures of both regioisomers

^aReactions were run on a 0.25 mmol scale with standard conditions; yield of the isolated product is reported as combined yields of both diastereomers, average of two runs; dr and rr were determined by NMR analysis of the unpurified mixture. *NMR yield.

product was preferentially formed when the substituent was in the 6- or 8-position on the phenyl ring (products 10-11). A lower yield was found for formation of 5 and 11, as coordination of the Lewis acid was likely impeded (see 12). X-ray structures of 13 and 14 were obtained to confirm the identity of the major regioisomer.

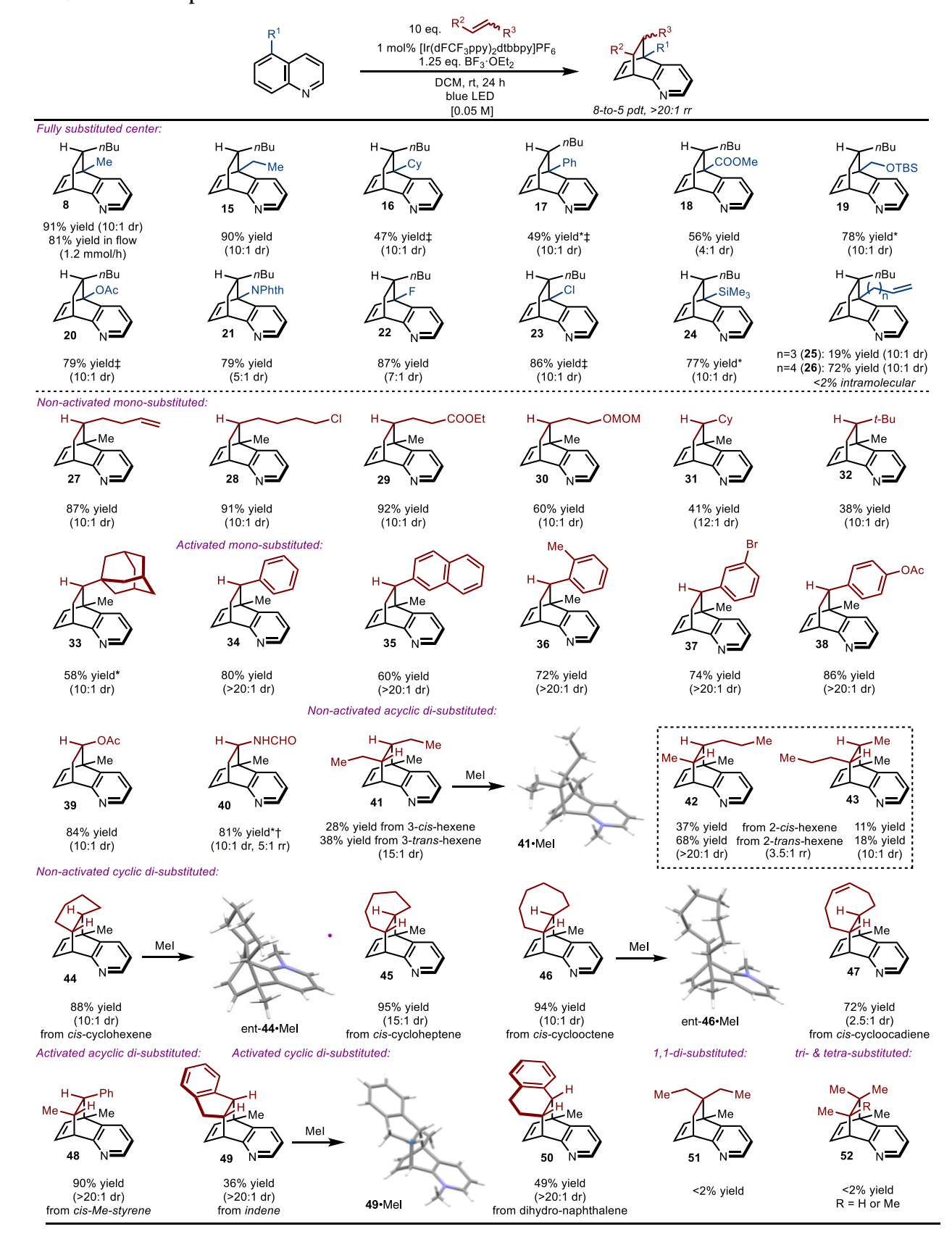
We explored the reaction scope for 5-substituted quinolines due to both the high diastereo- and regioselectivities observed and the potential for constructing products containing sterically congested carbons (Scheme 3). Substituents with a wide range of steric and electronic properties were well-tolerated under the conditions. Various quaternary carbons were achieved with different sp 3 (products 8, 15–16, 19) or sp 2 (products 17–18) substituted quinolines. Heteroatom substituted centers with F (product 22), Cl (product 23), O (product 20), N (product 21), and Si (product 24) were also easily prepared in high yields and selectivities. It is notable that intermolecular cycloaddition is faster than an intramolecular process (products 25–26). This is likely due to the slow reaction between C8 and the terminal carbon of the alkene via an 8- or 9-membered transition state. The alkene scope was also broad with excellent functional group compatibility with alkenes (product 27), ethers (product 30), esters (product 29), and halides (product 28). All monosubstituted alkenes, regardless if activated (products 34-40) or unactivated (products 27–33), favored formation of the endodiastereomer (dr \sim 10:1). Exclusive endo products (dr > 20:1) were found using styrenes regardless of the different substitution patterns. Even sterically demanding alkenes allowed for formation of the endo-products 31-33. With 1,2-disubstituted alkenes, stereo-convergence to the trans product was observed from either cis or trans alkene inputs (product 42-43), with the alkene substituent closer to the 5-position still being placed endo to the pyridine ring. Even for cis-cyclic alkenes like ciscyclohexene, cis-cycloheptene, and cis-cyclooctene, the trans products 44-46 were isolated with high diastereoselectivity. The anti-structures 41·MeI, 44·MeI, and 46·MeI were confirmed by X-ray analysis. The product of cis-cyclooctadiene 47 was formed with lower dr, presumably because bond rotation was constrained by the internal alkene. For indene and dihydronaphthalene, bond rotation was even more constrained, and only the cis-exo-isomers were isolated (49 and 50). With respect to limitations, 1,1-di, tri-, and tetrasubstituted alkenes did not allow for product formation (products 51-52). Finally, the reaction could be easily scaled up to 1.2 mmol/h using a flow chemistry system (8).

In addition to alkenes, allenes also underwent cycloadditions smoothly with quinoline substrates under standard conditions (Scheme 4, products 53-58).³² Regardless of the allene substitution pattern, the 8-to-5 product was exclusively formed. In the case of nonsymmetric allenes, mixtures of alkene isomers were formed (54 and 56). With 1,3-disubstituted allenes or trisubstituted allenes, the diastereoselectivities varied from endoto exo-selective (products 56–58).

Based on our previous report, 25 the mechanism of the reaction likely involves triplet-triplet energy transfer to a Lewis acidactivated quinoline followed by stepwise radical cycloaddition. However, there are several aspects that need to be considered in more detail (Scheme 5): (1) the role of the Lewis acid; (2) aromatic ring selectivity (benzene vs pyridine); (3) ortho, meta, and para selectivity; (4) 5-to-8 vs 8-to-5 regioselectivity; and (5) diastereoselectivity. We conducted further mechanistic studies to address all of these issues.

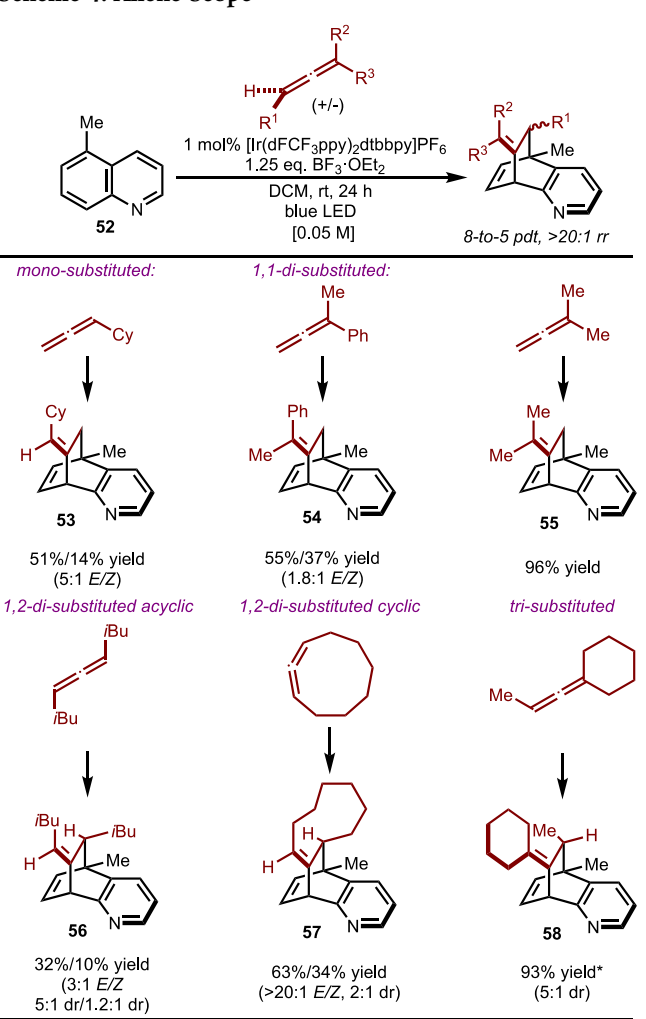
We first focused on determining the first nonreversible step of the reaction as it is important for understanding the origins of the observed selectivities. 33,34 To probe this, we conducted the standard reaction with the E- 2 D-labeled alkene **59**. If the intermolecular radical addition step was selectivity-determining,

Scheme 3. Substrate Scope^a



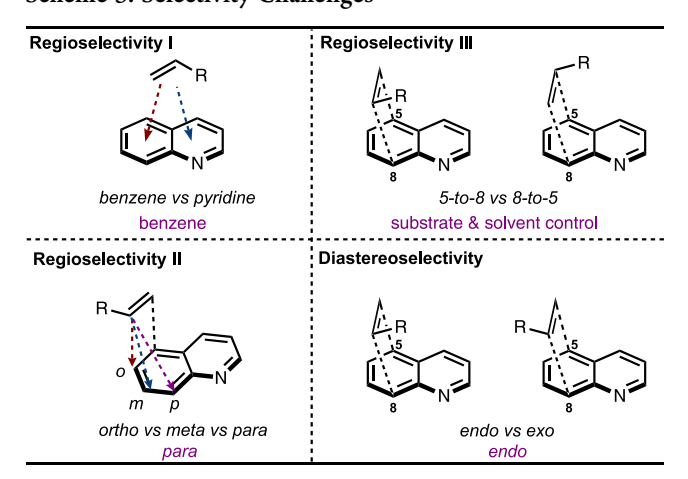
[&]quot;Reactions were run on a 0.25 mmol scale; yields of isolated products were reported as combined yields of both diastereomers; dr and rr were determined by NMR analysis of the unpurified mixture; average of two runs. Condition for methylation: MeI (5 equiv), dioxane, 50 °C, 12 h; *48 h; †yields of all for diastereo- and regioisomers; ‡>20:1 dr after purification.

Scheme 4. Allene Scope^a



^aReactions were run on a 0.25 mmol scale; values of dr, rr, and E/Z were determined by NMR analysis of the unpurified reaction mixture. *Combined yield of both diastereomers. Average of two runs.

Scheme 5. Selectivity Challenges



we would expect to isolate **60a** and/or **60b** with recovered unchanged **59** (Scheme 6A). However, while **60a** and **60b** were isolated in a 1:1 mixture, the excess unreacted alkene **59** was recovered as a 1:1 mixture of *E*- and *Z*-isomers. One interpretation of this result is if the first intermolecular radical

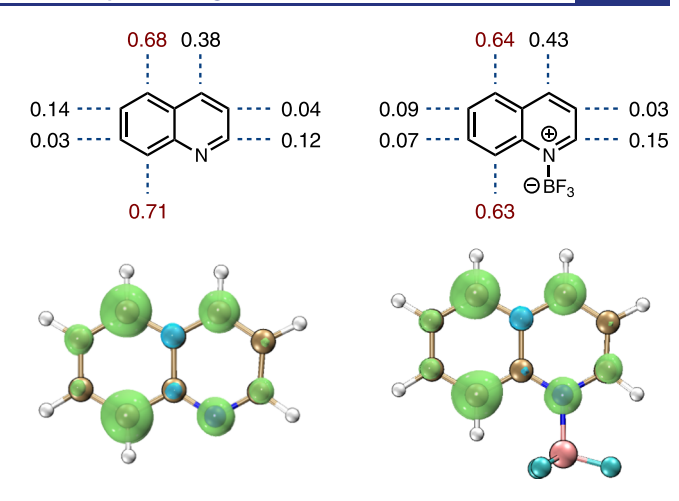


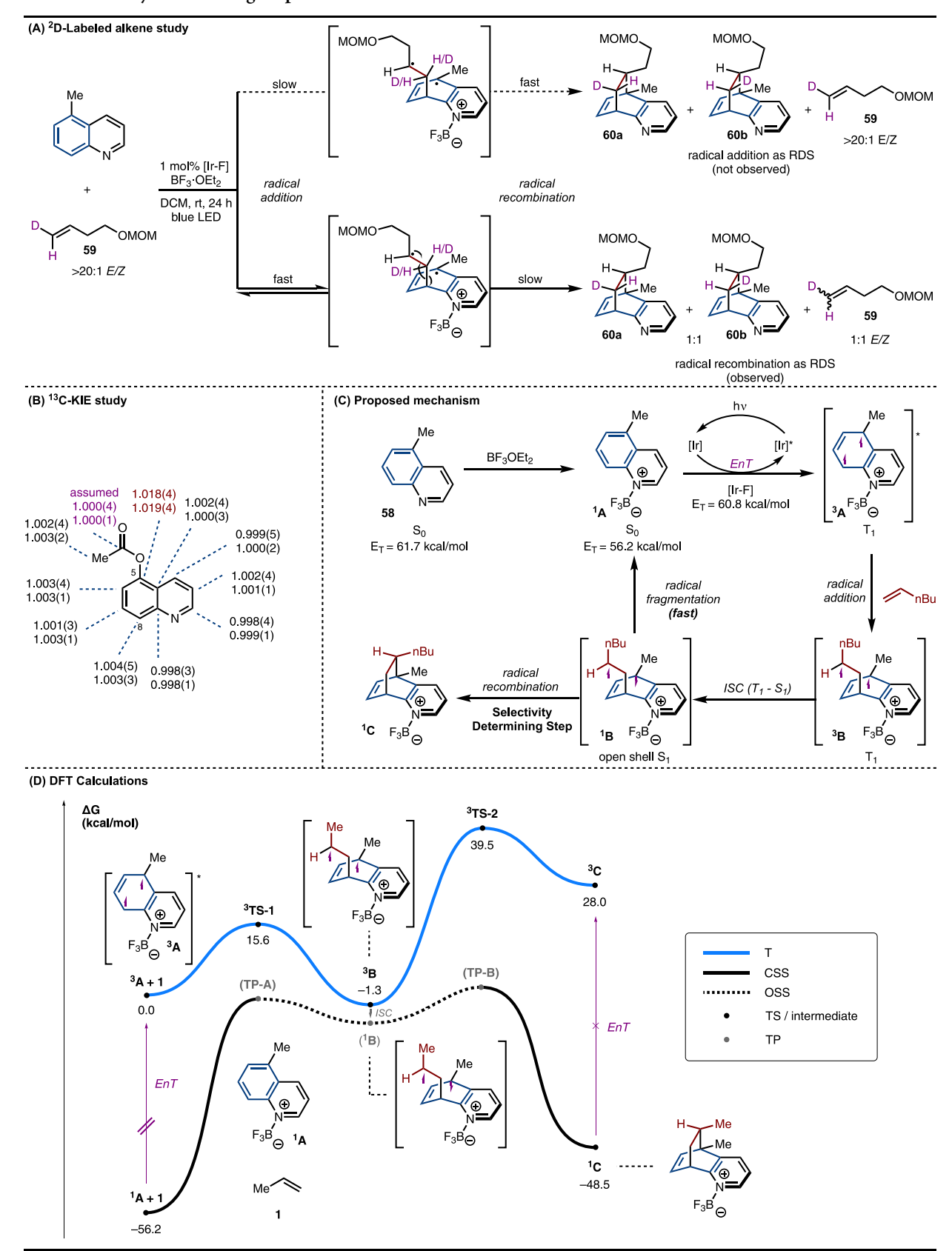
Figure 1. Calculated spin densities.

addition step is reversible and the second intramolecular radical recombination step is selectivity-determining. However, the isomerization of **59** could arise by an alternative unknown pathway. Therefore, ¹³C kinetic isotope effects (KIEs) at natural abundance were determined using the methods developed by Singleton and co-workers (Scheme 6B).³⁵ We initially carried out KIE measurements on 5-Me-quinoline, the standard substrate in all DFT calculations, and observed a strong KIE at C5 (1.017). However, overlapping signals in the ¹³C NMR spectra with C8 and C10 made it difficult to confirm the KIE value at C8. Thus, 5-OAc-quinoline was investigated and a similarly strong KIE at C5 was observed (1.019).

These mechanistic experiments strongly point to the first step being reversible and the intramolecular radical recombination being the selectivity-determining step. The observation that even *cis*-cyclic alkenes like cyclohexene preferentially form the *trans* product lends further support to the existence of a long-lived biradical intermediate that allows for bond rotation before recombination (see product 44, Scheme 3). A revised mechanism is therefore proposed in Scheme 6C. Photosensitization of the BF₃ complex ¹A by the excited triplet state of [Ir–F] generates ³A. Radical addition to 1-hexene then results in the formation of ³B, which upon intersystem crossing yields the singlet ¹B. This singlet intermediate can then undergo either radical fragmentation to revert to starting materials ¹A and 1-hexene or recombination to yield product ³C.

To further reveal the energetic landscape traversed by the reaction, which our experiments suggested was more complex than previously assumed, 25,38 we performed DFT calculations (Scheme 6D). The three energy surfaces, triplet (T), open-shell singlet (OSS), and closed-shell singlet (CSS), were mapped out in detail along the reaction coordinates. At the beginning of the reaction, energy transfer from the excited photosensitizer to the ground-state quinoline-BF₃¹A yields the triplet ³A. As the energy transfer process itself is not expected to impact the observed selectivities, we elected to focus our computational efforts on the subsequent transformations of ³A. Its reaction with propene (60) (used as a truncated computational model for 1hexene) via ³TS-1 on the triplet surface forms the first C-C bond with a calculated activation free energy of 15.6 kcal/mol. While the formation of the triplet biradical intermediate ³B is slightly exergonic, our calculations showed that it would most likely undergo intersystem crossing (ISC) to the open-shell singlet ¹B, which lies about 4–6 kcal/mol below ³B. The OSS and CSS surfaces intersect at two transition points (TPs) where

Scheme 6. Selectivity-Determining Step



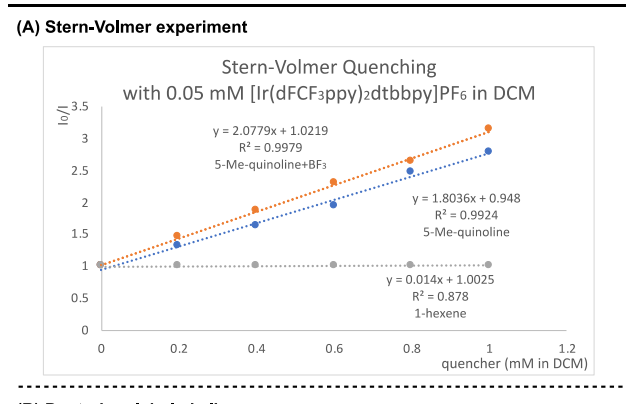
the open-shell and closed-shell wave functions transition smoothly: TP-A, which leads back to separated reactants, and TP-B, which furnishes the cycloadduct. Instead of being

determined by only a single triplet radical addition transition state (TS), the chemo- and diastereoselectivities of the reaction

are therefore controlled by the rate of ISC from ³B to ¹B, as well as the energies of the OSS to CSS **TPs**. ³⁶

Two possible roles were hypothesized for the requirement of Lewis acid complexation in this reaction: (1) facilitating energy transfer by lowering $E_{\rm T}$, and (2) accelerating the radical addition step by increasing the electrophilicity of the quinoline substrate. To probe the role of the Lewis acid in the energy transfer process, 37 we performed Stern–Volmer quenching studies. It was found that quinoline and quinoline–BF $_3$ complexes have similar quenching efficiencies (Scheme 7A). This result suggests

Scheme 7. Role of Lewis Acid



(B) Deuterium-labeled alkene

Me

I mol% [Ir-F]

OMOM

DCM, rt, 24 h
blue LED

DCM, rt, 24 h
blue LED

• Quinoline is sensitized, but radical addition to alkene does not occur

(C) Calculated free energy barriers (kcal/mol)

$$\begin{array}{c} \text{Me} \\ \text{Me} \\ \text{N} \\ \text{N} \\ \text{Me} \\ \text{N} \\ \text{Me} \\ \text{$$

that, while facilitating energy transfer, Lewis acid coordination is not strictly required for sensitization to happen. During the course of our study, Morofuji and Kano also showed that direct energy transfer to quinoline is feasible without the addition of an acid. 38,39 In contrast, the idea that Lewis acid primarily assists in the radical addition step found experimental support. When the standard reaction was conducted with E^{-2} D-labeled alkene **59** in the absence of BF₃, we observed <2% yield of the product and no epimerization of the alkene starting material, which indicated

that the radical addition barrier was significantly higher without the Lewis acid (Scheme 7B).

To further verify that Lewis and/or Brønsted acid complexation has the effect of lowering the radical addition barriers, we calculated the radical addition **TSs** between various quinoline substrates and alkene partners. In all cases, the calculations confirmed that both Lewis and Brønsted acid complexation led to lower activation free energies (ΔG^{\ddagger}) for the radical addition step (Scheme 7C). The magnitude of this effect is dependent on the identity of the acid as well as the quinoline/alkene combination, ranging from a 1.1 kcal/mol decrease for 5-Mequinoline/propene (with BF₃ complexation) to 5.3 kcal/mol for the 3-Me-quinoline/2-butene (with H⁺ complexation) system investigated by Morofuji and Kano.

Equipped with a deeper understanding of the reaction mechanism, we next sought to rationalize the observed selectivities. Our calculations of the triplet-state quinoline substrates indicate that there is a higher spin density on the benzene moiety than the pyridine moiety with or without Lewis acid complexation (Figure 1), which is likely linked to the experimentally observed regioselectivity for the benzene ring.

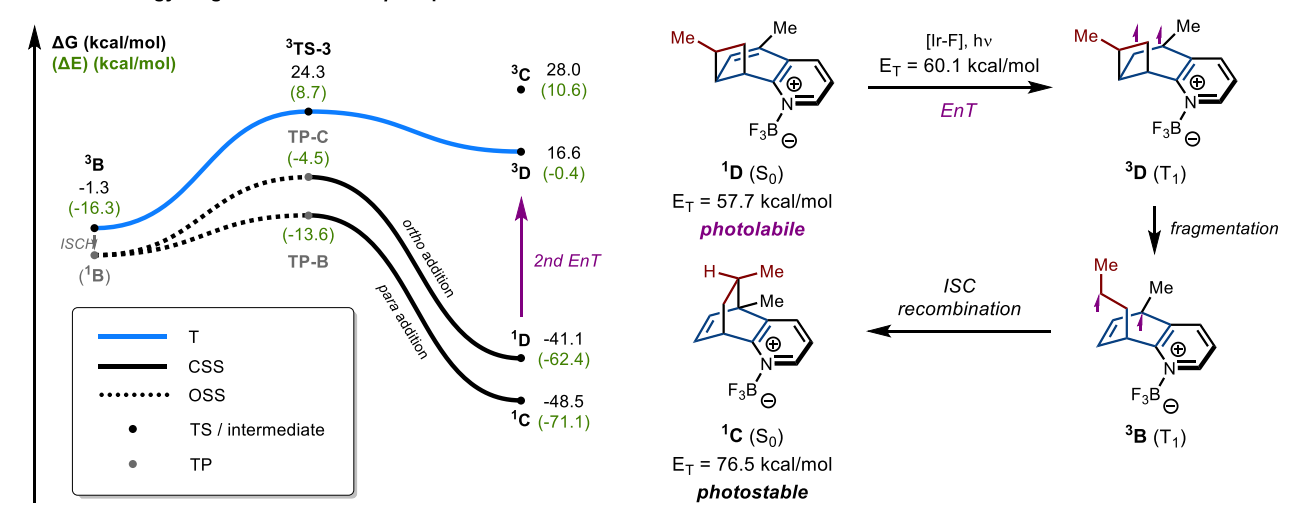
We next turned our attention to rationalizing the observed para selectivity of the reaction over ortho (meta cycloadditions were not considered here as they are concerted and occur exclusively on the singlet energy surface). As our mechanistic studies revealed that the OSS to CSS TPs were likely the selectivity-determining structures in the reaction, we concentrated our efforts on locating and comparing the TPs for the para and ortho addition pathways. Because free energies cannot be calculated for these **TPs** as thermal contributions to energy from molecular vibrations cannot be obtained for nonstationary points on the potential energy surface, 39 we present the electronic energies in Scheme 8A for the ortho- and paraadditions originating from ³B. We found that for both the TP and the final cycloadduct, the calculated electronic energies of ortho were much higher (9 kcal/mol) than para. This result suggests that the formation of the para cycloadduct is likely kinetically favorable for this substrate.

Furthermore, the *ortho* and *para* products also differ in their photostability under the reaction conditions. The $E_{\rm T}$ of the *ortho* product $^{\rm I}\mathbf{D}$ was calculated to be 57.7 kcal/mol, which is smaller than that of the photosensitizer [Ir–F] (60.1 kcal/mol). In contrast, the *para* product $^{\rm I}\mathbf{C}$ had a calculated $E_{\rm T}$ of 76.5 kcal/mol, meaning that it is likely photostable under the reaction conditions. We therefore reasoned that the *ortho* product can be sensitized and undergo radical fragmentation back to the starting materials, which funnels the reaction toward exclusive *para* product formation.

Although we were not able to isolate an *ortho* product and confirm the photosensitization-induced fragmentation, we observed two fused-ring products, which may suggest that an *ortho* cycloaddition does occur under the reaction conditions for certain substitution patterns (Scheme 8B).⁴⁰ Cyclopropyl chloride 66 was isolated together with the *para* cycloadduct 67. The formation of 66 can be rationalized through a second energy transfer to the *ortho* cycloadduct 62, followed by C–Cl bond homolysis.⁴¹ The resulting diradical 64 undergoes recombination to deliver 65. In addition, in the case of 68, a second energy transfer can occur to fragment the central C–C bond. Subsequent recombination can then yield a new cyclobutane product 73. Overall, while formation of the para adducts is likely kinetically favored, for some substitution patterns, a photolabile *ortho*-adduct may be generated.

Scheme 8. Ortho vs Para Selectivity

(A) Calculated energy diagram for ortho vs. para product formation



(B) Experimental evidence of second EnT

(a) 6-Cl-quinoline

Cl

BF3-OEt2

BF3-OEt2

Cl

N=

$$Cl$$

N=

 Cl

`nBu

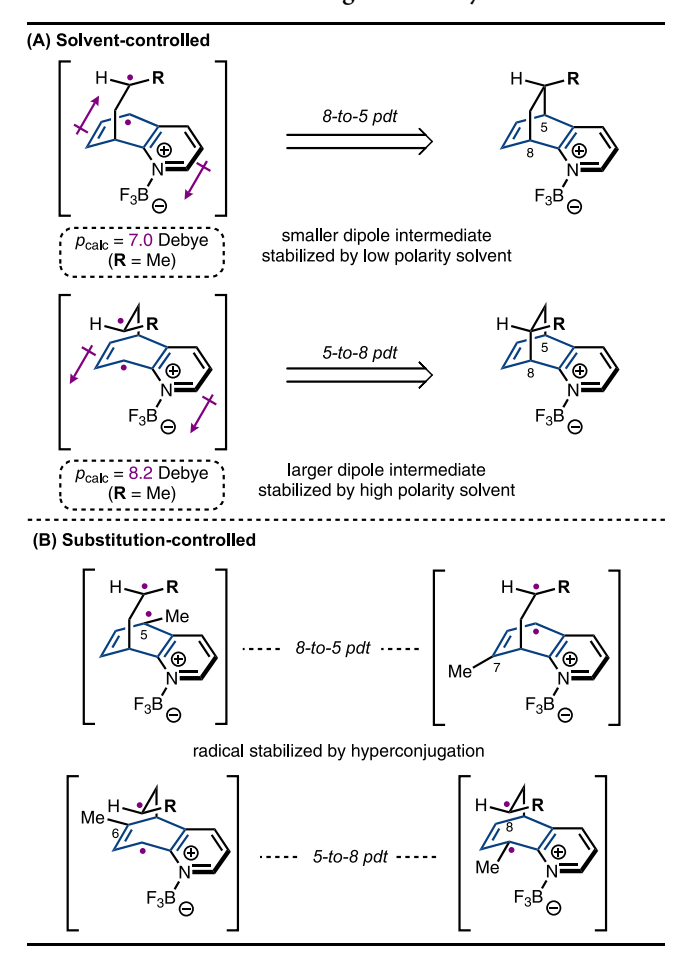
nBu

The 5-to-8 vs 8-to-5 regioselectivity of the reaction is also worthy of discussion. Having established through our mechanistic studies that the radical addition step is not selectivity-determining, we reasoned that the relative stability of the long-lived biradical intermediates could be key to explaining the regioselectivity. In the solvent-controlled regime (Scheme 2A), the biradical intermediate leading to the 5-to-8

CO₂Me

product is expected to have a larger net dipole moment due to the alignment of partial dipoles (Scheme 9A). As a result, the 5to-8 biradical intermediate would be better stabilized by more polar solvents. Our calculated dipole moment values (p_{calc}) for the biradical intermediates confirmed that the 5-to-8 biradical intermediate is more polar at 8.2 Debye, compared to 7.0 Debye for the 8-to-5 biradical intermediate. This is in good agreement

Scheme 9. 5-to-8 vs 8-to-5 Regioselectivity



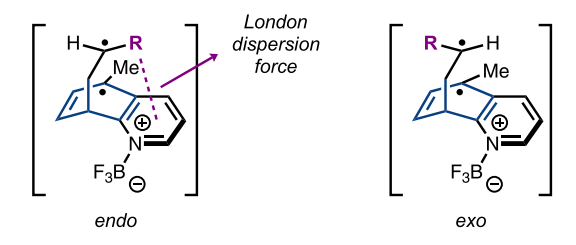
with our experimental observations that higher-polarity solvents favor the 5-to-8 product.

In the substitution-controlled regime (Scheme 2B), the stability of the biradical intermediates is primarily dictated by the degree of hyperconjugation. In these cases, the formation of the more stable biradical may render it less likely to undergo fragmentation back to starting materials. With an alkyl substituent in the 5- or 7-position, the biradical intermediate leading to the 8-to-5 product is better stabilized by hyperconjugative donation than its 5-to-8 counterpart (Scheme 9B). This explains the preferential formation of the 8-to-5 product for the 5- and 7-substituted substrates. For quinoline substrates with substitution in the 6- or 8-position, the 5-to-8 biradical intermediate would be better stabilized by hyperconjugation, leading to the opposite regioselectivity.

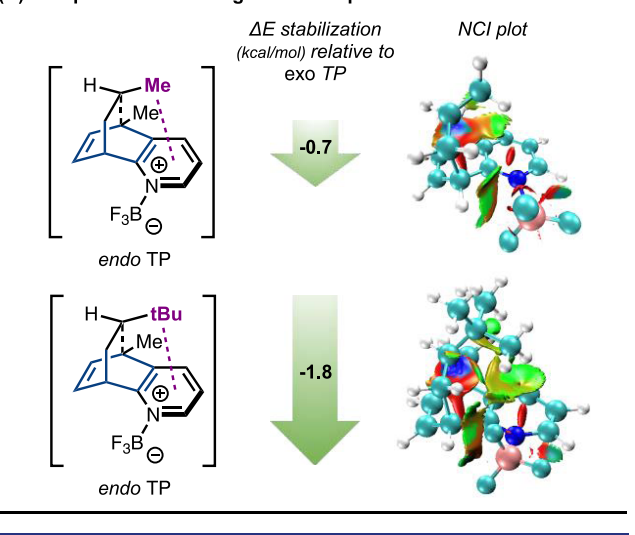
Finally, we set out to rationalize the *endo* diastereoselectivity of the reaction, for which we proposed that London dispersion forces could be the key factor (Scheme 10).⁴² To verify that dispersive interactions favor the formation of the *endo* product diastereomer, we compared TP energies calculated at the B3LYP/def2-TZVPP, SMD(CH₂Cl₂) (not dispersion-corrected), and B3LYP-D3/def2-TZVPP, SMD(CH₂Cl₂) (dispersion-corrected) levels (Scheme 10B). Our results confirmed that the electronic energies of the TPs leading to the *endo* diastereomers are indeed lowered more compared to the *exo* diastereomers when a dispersion-corrected functional was applied. In the reaction between 5-Me-quinoline and propene, dispersion correction favors the *endo*-product-forming TP by 0.7

Scheme 10. Endo vs Exo Diastereoselectivity

(A) London dispersion force



(B) Computational investigation of dispersion effects



kcal/mol relative to its *exo* counterpart. When the alkene substituent is a larger *tert*-butyl group instead of the methyl group of propene, this effect is even more pronounced, with dispersion adding 1.8 kcal/mol favorability to the *endo*-product-forming TP. Noncovalent interaction (NCI) plots for the MECPs also showed that at these C—C-forming bond lengths, the alkene substituent is within the right distance range to have favorable dispersive interactions with the pyridine moiety of the quinoline when in the *endo* position. These computational results showed that dispersion indeed has the effect of steering diastereoselectivity toward the *endo* product isomer.

CONCLUSIONS

We described herein a dearomative *para* -cycloaddition of quinolines with a variety of activated and unactivated alkenes. The reaction was enabled by photosensitization of the Lewis acid-complexed substrates and displays high diastereo- and regioselectivities that are tunable through varying the solvent and substitution patterns. Our mechanistic studies revealed a complex multisurface energetic landscape traversed by the reaction. Using a combined experimental and computational approach, we also disclosed the origins of the observed regio- and diastereoselectivities. Given the emerging interest in bridged polycycles and heterocycles in medicinal chemistry, we anticipate that this method will find substantial use in facilitating the efficient synthesis of such scaffolds.

ASSOCIATED CONTENT

Supporting Information

The Supporting Information is available free of charge at https://pubs.acs.org/doi/10.1021/jacs.2c07726.

Experimental procedures, analytical data for all new compounds (PDF)

Accession Codes

CCDC 2060640 and 2191096—2191099 contain the supplementary crystallographic data for this paper. These data can be obtained free of charge via www.ccdc.cam.ac.uk/data_request/cif, or by emailing data_request@ccdc.cam.ac.uk, or by contacting The Cambridge Crystallographic Data Centre, 12 Union Road, Cambridge CB2 1EZ, UK; fax: +44 1223 336033.

AUTHOR INFORMATION

Corresponding Authors

K. N. Houk — Department of Chemistry and Biochemistry, University of California, Los Angeles, Los Angeles, California 90095, United States; orcid.org/0000-0002-8387-5261; Email: houk@chem.ucla.edu

Frank Glorius — Organisch-Chemisches Institut, Westfälische Wilhelms-Universität Münster, 48149 Münster, Germany; orcid.org/0000-0002-0648-956X; Email: glorius@unimuenster.de

Shuming Chen – Department of Chemistry and Biochemistry, Oberlin College, Oberlin, Ohio 44074, United States;
orcid.org/0000-0003-1897-2249;
Email: shuming.chen@oberlin.edu

M. Kevin Brown — Department of Chemistry, Indiana University, Bloomington, Indiana 47405, United States; orcid.org/0000-0002-4993-0917; Email: brownmkb@indiana.edu

Authors

Renyu Guo – Department of Chemistry, Indiana University, Bloomington, Indiana 47405, United States

Souvik Adak – Department of Chemistry, Indiana University, Bloomington, Indiana 47405, United States

Peter Bellotti – Organisch-Chemisches Institut, Westfälische Wilhelms-Universität Münster, 48149 Münster, Germany

Xinfeng Gao – Department of Chemistry, Indiana University, Bloomington, Indiana 47405, United States

W. Walker Smith – Department of Chemistry, Indiana University, Bloomington, Indiana 47405, United States

Sam Ngan Le — Department of Chemistry and Biochemistry, Oberlin College, Oberlin, Ohio 44074, United States; orcid.org/0000-0002-1896-3038

Jiajia Ma – Organisch-Chemisches Institut, Westfälische Wilhelms-Universität Münster, 48149 Münster, Germany

Complete contact information is available at: https://pubs.acs.org/10.1021/jacs.2c07726

Notes

The authors declare no competing financial interest.

ACKNOWLEDGMENTS

The authors thank Indiana University and the NIH (R35GM131755) for financial support. This project was partially funded by the Vice Provost for Research through the Research Equipment Fund and the NSF MRI programs, CHE-1726633 and CHE-1920026. Support for the acquisition of the Bruker Venture D8 diffractometer through the Major Scientific Research Equipment Fund from the President of Indiana University and the Office of the Vice President for Research is gratefully acknowledged. S.C. is grateful to Oberlin College for financial support. DFT calculations were performed using the

SCIURus, the Oberlin College HPC cluster (NSF MRI 1427949). Generous financial support by the University of Munster and the Deutsche Forschungsgemeinschaft (SFB 858) is gratefully acknowledged.

REFERENCES

- (1) (a) Carruthers, W.; Baldwin, J. E. Cycloaddition Reactions in Organic Synthesis, Elsevier Science, 1990. (b) Kobayashi, S.; Jørgensen, K. A. Cycloaddition Reactions in Organic Synthesis; Wiley-VCH Verlag GmbH: Weinheim, Germany, 2001. (c) Nishiwaki, N. Methods and Applications of Cycloaddition Reactions in Organic Syntheses; John Wiley & Sons: New York, 2014.
- (2) (a) Ritchie, T. J.; Macdonald, S. J. F. The impact of aromatic ring count on compound developability are too many aromatic rings a liability in drug design? *Drug Discovery* **2009**, *14*, 1011–1020. (b) Lovering, F.; Bikker, J.; Humblet, C. Escape from Flatland: Increasing Saturation as an Approach to Improving Clinical Success. *J. Med. Chem.* **2009**, *52*, 6752–6756. (c) Lovering, F. Escape from Flatland 2: complexity and promiscuity. *Med. Chem. Commun.* **2013**, *4*, 515–519. (d) Mykhailiuk, P. K. Saturated bioisosteres of benzene: where to go next? *Org. Biomol. Chem.* **2019**, *17*, 2839–2849. (e) Subbaiah, M. A. M.; Meanwell, N. A. Bioisosteres of the Phenyl Ring: Recent Strategic Applications in Lead Optimization and Drug Design. *J. Med. Chem.* **2021**, *64*, 14046–14128.
- (3) For selected reviews see: (a) Streit, U.; Bochet, C. G. The Arene-Alkene Photocycloaddition. *Beilstein J. Org. Chem.* **2011**, *7*, 525–542. (b) Remy, R.; Bochet, C. G. Arene–Alkene Cycloaddition. *Chem. Rev.* **2016**, *116*, 9816–9849. (c) Okumura, M.; Sarlah, D. Visible-Light-Induced Dearomatizations. *Eur. J. Org. Chem.* **2020**, 2020, 1259–1273. (d) Cheng, Y.-Z.; Feng, Z.; Zhang, X.; You, S.-L. Visible-Light Induced Dearomatization Reactions. *Chem. Soc. Rev.* **2022**, *51*, 2145–2170.
- (4) Gilbert, A. The Inter- and Intramolecular Photocycloaddition of Ethylenes to Aromatic Compounds. *Pure Appl. Chem.* **1980**, *52*, 2669–2682.
- (5) Bryce-Smith, D. Orbital Symmetry Relationships for Thermal and Photochemical Concerted Cycloadditions to the Benzene Ring. *J. Chem. Soc. D* **1969**, 806–808.
- (6) Houk, K. N. Theory of Cycloadditions of Excited Aromatics to Alkenes. *Pure Appl. Chem.* **1982**, *54*, 1633–1650.
- (7) van der Hart, J. A.; Mulder, J. J. C.; Cornelisse, J. Funnels and barriers in the photocycloaddition of arenes to alkenes and dienes. *J. Photochem. Photobiol. A* **1995**, *86*, 141–148.
- (8) Cornelisse, J. The Meta Photocycloaddition of Arenes to Alkenes. *Chem. Rev.* **1993**, 93, 615–669.
- (9) (a) Wender, P. A.; Ternansky, R.; deLong, M.; Singh, S.; Olivero, A.; Rice, K. Arene-Alkene Cycloadditions and Organic Synthesis. *Pure Appl. Chem.* **1990**, *62*, 1597–1602. (b) Kärkäs, M. D.; Porco, J. A.; Stephenson, C. R. J. J. Photochemical Approaches to Complex Chemotypes: Applications in Natural Product Synthesis. *Chem. Rev.* **2016**, *116*, 9683–9747.
- (10) Anslyn, E. V.; Dougherty, D. A. Modern Physical Organic Chemistry; University Science Books: Sausalito, CA, 2006; Chapter 16, pp 935–1000.
- (11) El-Sayed, M. A. The Triplet State: Its Radiative and Nonradiative Properties. *Acc. Chem. Res.* **1968**, *1*, 8–16.
- (12) Wagner, P. J. Photoinduced Ortho [2 + 2] Cycloaddition of Double Bonds to Triplet Benzenes. *Acc. Chem. Res.* **2001**, *34*, 1–8.
- (13) (a) Mattay, J. Selectivities in Photocycloadditions of Arenes to Olefins. J. Photochem. 1987, 37, 167–183. (b) Stegbauer, S.; Jandl, C.; Bach, T. Enantioselective Lewis Acid Catalyzed ortho Photocycloaddition of Olefins to Phenanthrene-9-carboxaldehydes. Angew. Chem., Int. Ed. 2018, 57, 14593–14596.
- (14) (a) Döpp, D.; Krüger, C.; Memarian, H. R.; Tsay, Y.-H. 1,4-Photocycloaddition of α -Morpholinoacrylonitrile to 1-Acylnaphthalenes. *Angew. Chem., Int. Ed.* **1985**, *24*, 1048–1049. (b) Ohkura, K.; Sugaoi, T.; Sakushima, A.; Nishijima, K.; Kuge, Y.; Seki, K. Thermodynamically Controlled Photocycloaddition of 5-Fluoro-1,3-dimethyluracil to Naphthalenes. *Heterocycles* **2002**, *58*, 595–600.

- (15) For selected reviews, see: (a) Strieth-Kalthoff, F.; James, M. J.; Teders, M.; Pitzer, L.; Glorius, F. Energy transfer catalysis mediated by visible light: principles, applications, directions. *Chem. Soc. Rev.* **2018**, 47, 7190–7202. (b) Zhou, Q.-Q.; Zou, Y.-Q.; Lu, L.-Q.; Xiao, W.-J. Visible-Light-Induced Organic Photochemical Reactions through Energy-Transfer Pathways. *Angew. Chem., Int. Ed.* **2019**, 58, 1586–1604. (c) Strieth-Kalthoff, F.; Glorius, F. Triplet Energy Transfer Photocatalysis: Unlocking the Next Level. *Chem* **2020**, 6, 1888–1903. (d) Großkopf, J.; Kratz, T.; Rigotti, T.; Bach, T. Enantioselective Photochemical Reactions Enabled by Triplet Energy Transfer. *Chem. Rev.* **2022**, 122, 1626–1653.
- (16) Ma, J.; Schäfers, F.; Daniliuc, C.; Bergander, K.; Strassert, C. A.; Glorius, F. Gadolinium Photocatalysis: Dearomative [2 + 2] Cycloaddition/Ring-Expansion Sequence with Indoles. *Angew. Chem., Int. Ed.* **2020**, *59*, 9639–9645.
- (17) (a) Zhu, M.; Zheng, C.; Zhang, X.; You, S.-L. Synthesis of Cyclobutane-Fused Angular Tetracyclic Spiroindolines Via Visible-Light-Promoted Intramolecular Dearomatization of Indole Derivatives. *J. Am. Chem. Soc.* **2019**, *141*, 2636–2644. (b) Zhu, M.; Huang, X.-L.; Xu, H.; Zhang, X.; Zheng, C.; You, S.-L. Visible-Light-Mediated Synthesis of Cyclobutene-Fused Indolizidines and Related Structural Analogs. *CCS Chem.* **2020**, *2*, 652–664. (c) Zhu, M.; Zhang, X.; Zheng, C.; You, S.-L. Visible-Light-Induced Dearomatization via [2+2] Cycloaddition or 1,5-Hydrogen Atom Transfer: Divergent Reaction Pathways of Transient Diradicals. *ACS Catal.* **2020**, *10*, 12618–12626. (d) Zhu, M.; Huang, X.-L.; Sun, S.; Zheng, C.; You, S.-L. Visible-Light-Induced Dearomatization of Indoles/Pyrroles with Vinylcyclopropanes: Expedient Synthesis of Structurally Diverse Polycyclic Indolines/Pyrrolines. *J. Am. Chem. Soc.* **2021**, *143*, 13441–13449.
- (18) Oderinde, M. S.; Mao, E.; Ramirez, A.; Pawluczyk, J.; Jorge, C.; Cornelius, L. A. M.; Kempson, J.; Vetrichelvan, M.; Pitchai, M.; Gupta, A.; Gupta, A. K.; Meanwell, N. A.; Mathur, A.; Dhar, T. G. M. Synthesis of Cyclobutane-Fused Tetracyclic Scaffolds via Visible-Light Photocatalysis for Building Molecular Complexity. *J. Am. Chem. Soc.* **2020**, 142, 3094–3103.
- (19) Zhang, Z.; Yi, D.; Zhang, M.; Wei, J.; Lu, J.; Yang, L.; Wang, J.; Hao, N.; Pan, X.; Zhang, S.; Wei, S.; Fu, Q. Photocatalytic Intramolecular [2 + 2] Cycloaddition of Indole Derivatives via Energy Transfer: A Method for Late-Stage Skeletal Transformation. *ACS Catal.* **2020**, *10*, 10149–10156.
- (20) Zhuang, W.; Cheng, Y.-Z.; Huang, X.-L.; Huang, Q.; Zhang, X. Visible-Light Induced Divergent Dearomatization of Indole Derivatives: Controlled Access to Cyclobutane-Fused Polycycles and 2-Substituted Indolines. Org. Chem. Front. 2021, 8, 319–325.
- (21) Hu, N.; Jung, H.; Zheng, Y.; Lee, J.; Zhang, L.; Ullah, Z.; Xie, X.; Harms, K.; Baik, M.-H.; Meggers, E. Catalytic Asymmetric Dearomatization by Visible-Light-Activated [2 + 2] Photocycloaddition. *Angew. Chem., Int. Ed.* **2018**, *57*, 6242–6246.
- (22) Oderinde, M. S.; Ramirez, A.; Dhar, T. G. M.; Cornelius, L. A. M.; Jorge, C.; Aulakh, D.; Sandhu, B.; Pawluczyk, J.; Sarjeant, A. A.; Meanwell, N. A.; Mathur, A.; Kempson, J. Photocatalytic Dearomative Intermolecular [2 + 2] Cycloaddition of Heterocycles for Building Molecular Complexity. *J. Org. Chem.* **2021**, *86*, 1730–1747.
- (23) Strieth-Kalthoff, F.; Henkel, C.; Teders, M.; Kahnt, A.; Knolle, W.; Gómez-Suárez, A.; Dirian, K.; Alex, W.; Bergander, K.; Daniliuc, C. G.; Abel, B.; Guldi, D. M.; Glorius, F. Discovery of Unforeseen Energy-Transfer-Based Transformations Using a Combined Screening Approach. *Chem* **2019**, *5*, 2183–2194.
- (24) (a) Kishikawa, K.; Akimoto, S.; Kohmoto, S.; Yamamoto, M.; Yamada, K. Intramolecular photo [4+2] cycloaddition of an enone with a benzene ring. *J. Chem. Soc., Perkin Trans.* 1 1997, 77–84. (b) Ma, J.; Strieth-Kalthoff, F.; Dalton, T.; Freitag, M.; Schwarz, J. L.; Bergander, K.; Daniliuc, C.; Glorius, F. Direct Dearomatization of Pyridines via an Energy-Transfer-Catalyzed Intramolecular [4 + 2] Cycloaddition. *Chem* 2019, 5, 2854–2864.
- (25) Ma, J.; Chen, S.; Bellotti, P.; Guo, R.; Schafer, F.; Heusler, A.; Zhang, X.; Daniliuc, C.; Brown, M. K.; Houk, K. N.; Glorius, F. Photochemical intermolecular dearomative cycloaddition of bicyclic azaarenes with alkenes. *Science* **2021**, *371*, 1338–1345.

- (26) (a) Taylor, R. D.; MacCoss, M.; Lawson, A. D. Rings in Drugs. *J. Med. Chem.* **2014**, *57*, 5845–5859. (b) Vitaku, E.; Smith, D. T.; Njardarson, J. T. Analysis of the Structural Diversity, Substitution Patterns, and Frequency of Nitrogen Heterocycles among U.S. FDA Approved Pharmaceuticals. *J. Med. Chem.* **2014**, *57*, 10257–10274. (c) Blakemore, D. C.; Castro, L.; Churcher, I.; Rees, D. C.; Thomas, A. W.; Wilson, D. M.; Wood, A. Organic Synthesis Provides Opportunities to Transform Drug Discovery. *Nat. Chem.* **2018**, *10*, 383–394.
- (27) (a) Ma, J.; Chen, S.; Bellotti, P.; Wagener, T.; Daniliuc, C.; Houk, K. N.; Glorius, F. Facile access to fused 2D/3D rings via intermolecular cascade dearomative [2 + 2] cycloaddition/rearrangement reactions of quinolines with alkenes. *Nat. Catal.* **2022**, *5*, 405–413. (b) Bellotti, P.; Rogge, T.; Paulus, F.; Laskar, R.; Rendel, N.; Ma, J.; Houk, K. N.; Glorius, F. Visible-Light Photocatalyzed *peri*-(3 + 2) Cycloadditions of Quinolines. *J. Am. Chem. Soc.* **2022**, *144*, 15662–15671.
- (28) Elliott, L. D.; Kayal, S.; George, M. W.; Booker-Milburn, K. Rational Design of Triplet Sensitizers for the Transfer of Excited State Photochemistry from UV to Visible. *J. Am. Chem. Soc.* **2020**, *142*, 14947–14956.
- (29) Reichardt, C.; Welton, T. Solvents and Solvent Effects in Organic Chemistry, 3rd ed.; Wiley-VCH Publishers, 2003; pp 470–475.
- (30) During the investigation we found it necessary to switch from the optimized solvent PhMe to CH_2Cl_2 , and to dilute the reaction to [0.05 M] for improved solubility (especially for substituted quinolines).
- (31) Chénard, E.; Sutrisno, A.; Zhu, L.; Assary, R. S.; Kowalski, J. A.; Barton, J. L.; Bertke, J. A.; Gray, D. L.; Brushett, F. R.; Curtiss, L. A.; Moore, J. S. Synthesis of Pyridine— and Pyrazine—BF₃ Complexes and Their Characterization in Solution and Solid State. *J. Phys. Chem. C* **2016**, *120*, 8461—8471.
- (32) For photochemical reaction with allenes, see: (a) Haddaway, K.; Somekawa, K.; Fleming, P.; Tossell, J. A.; Mariano, P. S. Chemistry of Allene Cation Radicals Probed by the Use of Theoretical and Electrontransfer Photochemical Methods. *J. Org. Chem.* 1987, 52, 4239–4253. (b) Birbaum, F.; Neels, A.; Bochet, C. G. Photochemistry of Allenyl Salicylaldehydes. *Org. Lett.* 2008, 10, 3175–3178. (c) Streit, U.; Birbaum, F.; Quattropani, A.; Bochet, C. G. Photocycloaddition of Arenes and Allenes. *J. Org. Chem.* 2013, 78, 6890–6910.
- (33) Several previous studies have proposed that the first step is the selectivity determining step. See refs 19, 22, 23.
- (34) For a recent study that highlights a selectivity determining radical recombination, see Zhu, M.; Zheng, C. Post-Spin Crossing Dynamics Determine the Regioselectivity in Open-Shell Singlet Biradical Recombination. *Org. Chem. Front.* **2022**, *9*, 995–1003.
- (35) (a) Singleton, D. A.; Thomas, A. A. High-Precision Simultaneous Determination of Multiple Small Kinetic Isotope Effects at Natural Abundance. *J. Am. Chem. Soc.* **1995**, *117*, 9357–9358. (b) Beno, B. R.; Houk, K. N.; Singleton, D. A. Synchronous or Asynchronous? An "Experimental" Transition State from a Direct Comparison of Experimental and Theoretical Kinetic Isotope Effects for a Diels—Alder Reaction. *J. Am. Chem. Soc.* **1996**, *118*, 9984–9985. (c) Hirschi, J. S.; Takeya, T.; Hang, C.; Singleton, D. A. Transition State Geometry Measurements from ¹³C Isotope Effects. The Experimental Transition State for the Epoxidation of Alkenes with Oxaziridines. *J. Am. Chem. Soc.* **2009**, *131*, 2397–2403. (d) For ¹³C KIE at natural abundance to probe a photochemical reaction, see: Kuan, K.-Y.; Singleton, D. A. Isotope Effects and the Mechanism of Photoredox-Promoted [2 + 2] Cycloadditions of Enones. *J. Org. Chem.* **2021**, *86*, 6305–6313.
- (36) It is also possible that the trajectory of approach of the alkene to the triplet quinoline diradical may influence the selectivity.
- (37) Daub, M. E.; Jung, H.; Lee, B. J.; Won, J.; Baik, M.-H.; Yoon, T. P. Enantioselective [2+2] Cycloadditions of Cinnamate Esters: Generalizing Lewis Acid Catalysis of Triplet Energy Transfer. *J. Am. Chem. Soc.* **2019**, *141*, 9543–9547.
- (38) Morofuji, T.; Nagai, S.; Chitose, Y.; Abe, M.; Kano, N. Protonation-Enhanced Reactivity of Triplet State in Dearomative Photocycloaddition of Quinolines to Olefins. *Org. Lett.* **2021**, 23, 6257–6261. The free energy barriers shown in Scheme 7C were recalculated and differ from those calculated by the original authors.

- (39) Gaussian 16 Users Reference, Keyword: Freq, 2021. https:// gaussian.com/man/.
- (40) (a) see ref 27. (b) Zhu, M.; Xu, H.; Zhang, X.; Zheng, C.; You, S.-L. Visible-Light-Induced Intramolecular Double Dearomative Cycloaddition of Arenes. Angew. Chem., Int. Ed. 2021, 60, 7036-7040.
- (41) For triplet radical H atom abstraction, see: (a) ref 27 (b) Xiong, Y.; Großkopf, J.; Jandl, C.; Bach, T. Visible Light-Mediated Dearomative Hydrogen Atom Abstraction/Cyclization Cascade of Indoles. Angew. Chem., Int. Ed. 2022, 61, No. e202200555.
- (42) For selected reviews, see: (a) Krenske, E. H.; Houk, K. N. Aromatic Interactions as Control Elements in Stereoselective Organic Reactions. Acc. Chem. Res. 2013, 46, 979-989. (b) Wagner, J. P.; Schreiner, P. R. London Dispersion in Molecular Chemistry-Reconsidering Steric Effects. Angew. Chem., Int. Ed. 2015, 54, 12274-12296. (c) Wheeler, S. E.; Seguin, T. J.; Guan, Y.; Doney, A. C. Noncovalent Interactions in Organocatalysis and the Prospect of Computational Catalyst Design. Acc. Chem. Res. 2016, 49, 1061–1069. (d) Grimme, S.; Hansen, A.; Brandenburg, J. G.; Bannwarth, C. Dispersion-Corrected Mean-Field Electronic Structure Methods. Chem. Rev. 2016, 116, 5105-5154. (e) Bursch, M.; Caldeweyher, E.; Hansen, A.; Neugebauer, H.; Ehlert, S.; Grimme, S. Understanding and Quantifying London Dispersion Effects in Organometallic Complexes. Acc. Chem. Res. 2019, 52, 258-266. (f) Pollice, R.; Chen, P. A Universal Quantitative Descriptor of the Dispersion Interaction Potential. Angew. Chem., Int. Ed. 2019, 58, 9758-9769.

□ Recommended by ACS

Polyarylquinone Synthesis by Relayed Dehydrogenative [2 + 2 + 2] Cycloaddition

Soumyadip Hore, Ravi P. Singh, et al.

MAY 10 2022 ACS CATALYSIS

READ 2

Insights into the Mechanism of an Allylic Arylation Reaction via Photoredox-Coupled Hydrogen Atom Transfer

Ethan H. Spielvogel, John R. Swierk, et al.

DECEMBER 09, 2021

THE JOURNAL OF ORGANIC CHEMISTRY

READ **C**

Copper-Catalyzed Three-Component Germyl Peroxidation of Alkenes

Yani Luo, Zhiping Li, et al.

MARCH 18, 2022 ORGANIC LETTERS

READ **C**

Photoinduced B-Cl Bond Fission in Aldehyde-BCl₃ Complexes as a Mechanistic Scenario for C-H Bond Activation

Daniel P. Schwinger, Thorsten Bach, et al.

OCTOBER 07, 2022

JOURNAL OF THE AMERICAN CHEMICAL SOCIETY

READ **C**

Get More Suggestions >